Structural Engineering and Mechanics, Vol. 18, No. 5 (2004) 691-707
DOI: http://dx.doi.org/10.12989/sem.2004.18.5.691

Micro-mechanical modeling for compressive behavior of concrete material

P. Haleerattanawattana†, T. Senjuntichai‡ and E. Limsuwan‡†

Department of Civil Engineering, Chulalongkorn University, Bangkok 10330, Thailand

(Received June 3, 2003, Accepted July 23, 2004)

Abstract. This paper presents the micro-mechanical modeling for predicting concrete behavior under compressive loading. The model is able to represent the heterogeneities in the microstructure up to three phases, i.e., aggregate particles, matrix and interfaces. The smeared crack concept based on non-linear fracture mechanics is implemented in order to formulate the constitutive relation for each component. The splitting tensile strength is considered as a fracture criterion for cracking in micro-level. The finite element method is employed to simulate the model based on plane stress condition by using quadratic triangular elements. The validation of the model is verified by comparing with the experimental results. The influence of tensile strength from both aggregate and matrix phases on the concrete compressive strength is demonstrated. In addition, a guideline on selecting appropriate tensile strength for each phase to obtain specified concrete compressive strength is also presented.

Key words: micro-mechanical modeling; finite element method; non-linear fracture mechanics; concrete material; compressive behavior.

1. Introduction

It is well known that the concrete material is a complex mixture composed of various components with different characteristics. The properties of the material vary from one position to another. It is very difficult to establish a general theory describing the overall concrete response from micro-structural aspect. However, if such principle is developed, the mechanical behavior of concrete can be predicted. In addition, suitable materials can then be selected to produce concrete with specified performance. The literature review indicates that the available micro-mechanical models for concrete can be grouped into two categories; discrete element method and continuum element method.

The discrete element method is based on a special assembly of specific elements to simplify the problem. This type of models has been classified into two groups based on the underlying principle, i.e., the particle model and the lattice model. For the former, Zubelewicz and Bazant (1987) developed the interface element to simulate cracks in composites of rigid inclusions embedded in a soft linear elastic matrix. The interface layer cracking was based on the strength criterion of normal force component. Consequently, the softening stress-strain relation after peak load corresponding to

† Ph.D. Student
‡ Assistant Professor
‡† Professor

the microscopic interparticle fracture energy was introduced by Bazant *et al*. (1990). In their paper, the truss network model is employed to exhibit the size effect of specimens. While, Schlangen and van Mier (1992) adopted the lattice model of beam elements to simulate the brittle behavior of a concrete material. Recently, Zhong and Chang (1999) proposed the discrete element model by assuming that the interparticle binder initially contains microcracks. The stress-strain behaviors under uniaxial and biaxial conditions were presented.

In the continuum element approach, regular types of elements are used to represent the entire domain of concrete. Thus, they can easily be implemented into a common finite element program. The special attention has been directed toward the development of the constitutive relation that takes into account the non-linearity of material. Roelfstra (1989) considered the elastic aggregate particles connecting to the weaker matrix phase by softening springs and friction elements. By employing the concept of linear elastic fracture mechanics, Zaitsev and Wittmann (1981) simulated crack propagation and failure of concrete and hardened cement paste. The crack trajectories of the granular microcracked concrete body under direct tension were numerically investigated by Wang *et al*. (1993). Bazant and Oh (1983) introduced the idea of crack band model in the smeared sense to present the continuously distributed microcracking within a fixed width. The concept of smeared crack is also implemented in the truss-network model by Mohamed and Hansen (1999a, b) to simulate the crack patterns of concrete specimen under different types of loading. In their model, the tensile cracking at the micro-level is the failure criterion and only axial deformation is considered in the forms of truss elements, i.e., shear deformation is neglected.

In the context of three-dimensional analysis, Bazant *et al*. (1996) implemented the microplane model to investigate nonlinear tri-axial behavior of concrete in compression with shear. Although the microstructure of concrete is actually three-dimensional, the two-dimensional modeling can represent the global behavior of concrete material satisfactorily with much less effort and time-consuming when compared to a rigorous three-dimensional analysis.

In this paper, a simple model of concrete microstructure for predicting concrete behavior under compressive loading is presented. The finite element model is generated based on the two-dimensional plane stress condition by using quadratic triangular elements. Shear deformation is thus included in the model. The concrete cracking and constitutive relation come from the concept of non-linear fracture mechanics. The failure criterion is applied to all three phases, i.e., aggregate, matrix, and interfaces. The accuracy of the proposed model is verified by comparing with the experimental results. The influence of tensile strength from both aggregate and mortar phases on concrete compressive strength is studied. In addition, a simple chart for selecting an appropriate tensile strength of each phase for desired compressive strength of concrete is established.

2. Micro-mechanical model for concrete

2.1 Heterogeneity simulation

The microstructure of concrete is too complex. It includes several inhomogeneities that widely vary in their size. For example, the general dimension of coarse aggregate is more than 10 mm, while a fine aggregate scales from 0.01 to 10 mm. The capillary pores embedded in the nanometer structure of hydration products are about 0.0005-0.01 mm. Therefore, it is impossible to model the entire microstructure of concrete by a single model. Zaitsev and Wittmann (1981) suggested

Table 1 Structural levels of concrete and corresponding features

Structural level	Macro-level	Meso-level	Micro-level	Nana-level
Main heterogeneity	Coarse aggregate	Fine aggregate	Large pores	Small pores
Order or RVE*	over 100 mm.	0.1 to 10 mm.	5e-4 to 0.01 mm.	under 5e-4 mm.
Stress-strain characteristic	Non-linear	Quasi-linear	Approx. linear	Linear
Type of models	Structural eng.	Material eng.	Material science	Material science

RVE* is the representative volume element.

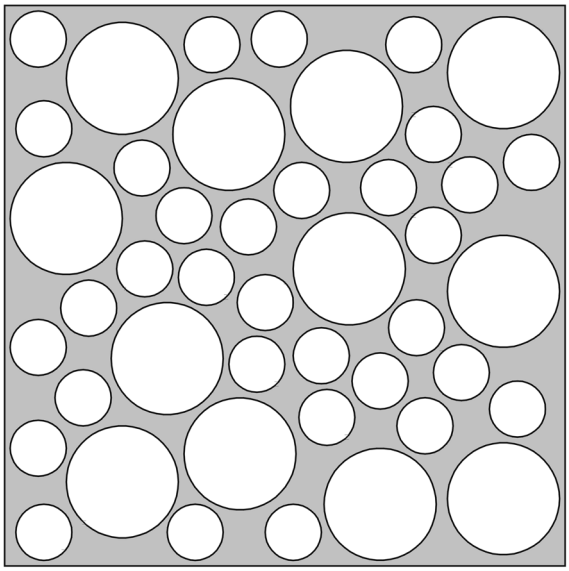

Fig. 1 Geometry of concrete microstructure considered in this study

considering concrete microstructure as a multi-level hierarchy system. Concrete is composed of the random inclusions of coarse aggregate in a homogeneous mortar, which can be modeled further as a system of distributed fine aggregate particles in a matrix of cement paste. Moreover, cement paste comprises of pore space in uniform mass of hydration products. The important characteristics for each level are summarized in Table 1.

In this study, the internal structure of concrete is idealized as reinforced with randomly distributed round inclusions in the matrix system. The sample of the internal geometry is shown in Fig. 1. The circles may represent coarse aggregate particles, fine aggregate grains or pore spaces, depending on the level of observation. This inclusion phase is generated according to a given particle size distribution. The simulation procedure of inclusion is similar to the one employed previously by Bazant *et al*. (1990). The minimum clearance of 0.5 mm between the particles, the boundaries, and 1 mm among the particles are established to provide space for the matrix phase to surround the inclusion particles, and to prevent the particle overlapping.

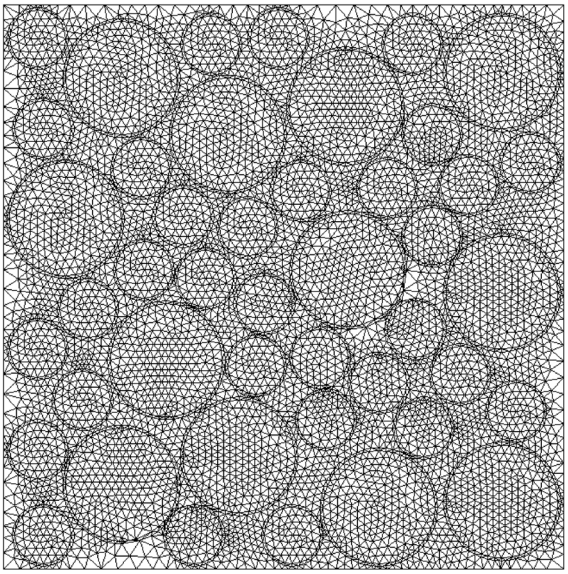

Fig. 2 Mesh generation for concrete microstructure

2.2 Finite element modeling

The analysis of a micro-mechanical model for concrete, like in Fig. 1, requires the application of numerical methods. In this paper, the continuum finite element method is selected to be a tool for handling such a model. The finite element mesh for a system is generated based on Delaunay triangulation. The sample mesh generation of concrete microstructure is shown in Fig. 2. The ring areas around aggregate particles represent the interface phase.

For the sake of simplicity, the plane stress condition is assumed, and the quadratic triangular elements with straight sides and midside nodes are employed for the discretization. This element is considered an excellent element for two-dimensional analysis (Cook *et al*. 2002). The stiffness matrix for quadratic triangular element can be expressed as

$$[k] = \int_V [B]^T [E][B] dV \tag{1}$$

where $[B]$ is the strain-displacement matrix and $[E]$ denotes the constitutive matrix. For isotropy and plane stress condition, $[E]$ can be given by

$$[E] = \frac{E}{(1+\nu)(1-2\nu)} \begin{bmatrix} 1-\nu & \nu & 0 \\ \nu & 1-\nu & 0 \\ 0 & 0 & \dfrac{1-2\nu}{2} \end{bmatrix} \tag{2}$$

where E is the elastic modulus, and ν is Poisson's ratio.

2.3 Failure criterion and constitutive relation

In the macro-level, a concrete member subjected to any type of loading may fail due to the effect of splitting, crushing, shearing, or the combination of these actions depending on size, shape and boundary condition of the specimen (Kotsovos 1987). However, from the micro-structural point of view, it is accepted that the failure of concrete is the result of the initiation, propagation and coalition of individual cracks. These cracks normally occur when the principal tensile stress of the element in the material reaches the value of tensile strength of the material (Bangash 1989). The plane of tensile strength depends on loading and boundary conditions. Thus, the present model is based on the hypothesis that cracking at the micro-level of concrete material is a failure criterion, and the tensile strength is a key parameter.

When the loading is initially applied to the specimen, the principal stress within each element does not reach the tensile strength of the material. All elements throughout the specimen behave like linear elastic materials, and the constitutive matrix ($[E]$) for the plane stress condition given in Eq. (2) can be used. However, when the load is higher and tensile stress in the element reaches the tensile strength, a crack is then taken place and the constitutive matrix is changed. According to Karihaloo (1995), the stiffness matrix under plane stress condition for the element that the crack occurs can be expressed as

$$[E] = \begin{bmatrix} E & 0 & 0 \\ 0 & E' & 0 \\ 0 & 0 & \dfrac{E\beta}{(1+\nu)} \end{bmatrix} \tag{3}$$

where E is the secant elastic modulus of the element, E' is the slope of stress-strain curve after peak, as shown in Fig. 3, and β is the shear retention factor. In this model, the value of β that equals 0.4 is used (Lorrain *et al*. 1999).

From the constitutive matrix of the element after cracking given in Eq. (3), it is implied that an element under compression is linear elastic throughout the simulations. On the other hand, the

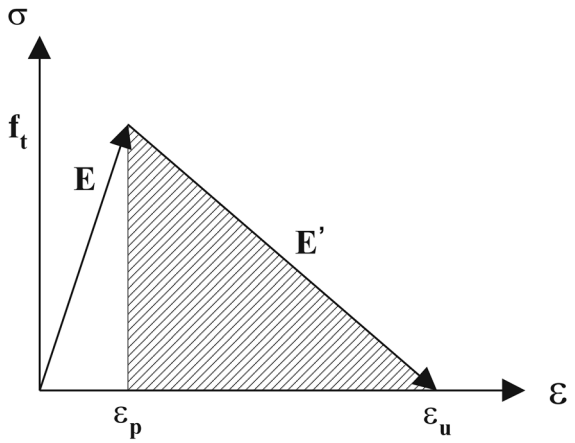

Fig. 3 Constitutive relation for element subjected to tension

stress-strain relation for elements subjected to tension is linear elastic up to the splitting tensile strength (f_t), and then is followed by a softening part, as shown by a shaded area in Fig. 3. Therefore, the parameters required to establish the first part of the relation are E, f_t, and ν. The parameter associated with the softening part of the curve is the fracture energy associated with the given shape of stress-separation curve (G_F). This parameter can be derived from the concepts of non-linear fracture mechanics, which are described in the following subsection.

2.4 Fracture toughness of concrete

The fracture energy or fracture toughness (G) is the required energy for the propagation of a unit length of crack in a material with unit thickness (Shah *et al.* 1995). For a concrete material that behaves like a quasi-brittle material, the fracture energy is divided into two parts: (i) the energy consumed to create new crack surface, and (ii) the energy to overcome the cohesive pressure in fracture process zone to separate the surfaces. However, the fictitious crack approach considers the former energy to be negligible when compared to the latter one. Then the fracture energy can be expressed as

$$G = \int_0^{w_t} \sigma(w)\,dw \tag{4}$$

where $\sigma(w)$ is the normal cohesive pressure defined as a function of separation displacement and w_t is the crack separation displacement at the initial crack tip, as shown in Fig. 4. The cohesive pressure is equal to tensile strength (f_t) of the material where the microcrack starts and zero at the crack tip. The upper limit of the integration w_t will become the critical crack separation (w_c) for full crack separation (Shah *et al.* 1995). Accordingly, the integration in Eq. (4) for the area under entire softening stress-strain curve is given by

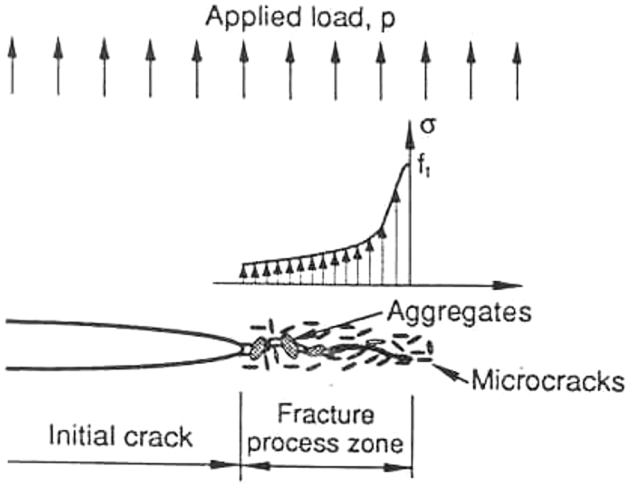

Fig. 4 Concrete crack and cohesion pressure in fracture process zone (Shah *et al.* 1995)

$$G_F = \int_0^{w_c} \sigma(w)dw \tag{5}$$

By assuming linear decay of stress-separation curve, Eq. (5) becomes

$$w_c = \frac{2G_F}{f_t} \tag{6}$$

According to the idea of smeared crack presented by Bazant and Oh (1983), the ultimate strain ε_u of an element can be computed from w_c in Eq. (6) by introducing a parameter of element size (h_c) as

$$\varepsilon_u = \frac{w_c}{h_c} \tag{7}$$

The term "element size" seems ambiguous in this model since the triangular element is used. However, it helps the model to be independent of the mesh number and the specimen scale (Bazant and Planas 1998). In this paper, the element size is assumed to be a function of the element area, which will be evaluated in the calibration step.

2.5 Calibration for element size

Since the element size (h_c) is incorporated in the model, the calibration is then performed to determine the value of h_c based on the axial elastic modulus testing. This procedure is similar to the one used by Mohamed and Hansen (1999a) for the truss-network model. First, the element size is assumed to be the ratio of the element area, and the same elastic modulus is assigned to all elements in the specimen. A unit deformation is applied at one end, while the other end is fixed in the loading direction and free in the perpendicular direction. After evaluating the reaction at the fixed end, the resulting elastic modulus of the specimen can be computed. If it is different from the previous value, the calculation is repeated with a new element size being given until the computed elastic modulus agrees well with the assigned one. It is found that the ratio between the element size and the element area is different when the inclusion arrangement pattern is changed. The ratio is varied from 0.68 to 0.84. Nevertheless, this ratio is quite constant with respect to the mesh size.

3. Model prediction for compressive loading

Consider a 100 × 100-mm concrete specimen subjected to compressive loading. The aggregate particles are distributed exactly as shown in Fig. 1. Two sizes of the aggregate are used, i.e., 10 and 20 mm in the ratio of 60:40 by area. The aggregate particles occupy about 64% of the whole specimen area. The material properties for each phase are given in Table 2. In the first simulation, the interface phase is neglected by assigning the same properties as those of the bulk paste. For two other cases, the interface phase is considered with the properties, except Poisson's ratio, being less than those of the bulk paste.

All simulations for compression test are performed by gradually applying a uniform displacement at one end, while the other end is prevented from movements in loading direction but is free in the

Table 2 Material properties of each phase for the numerical result in Fig. 5

Phase	Simulation	E (GPa)	f_t (MPa)	G_F (N/mm)	ν
Aggregate	All	80	16.0	0.080	0.15
Matrix	All	40	8.0	0.064	0.25
Interface	1	40	8.0	0.064	0.25
	2	36	7.2	0.058	0.25
	3	32	6.4	0.051	0.25

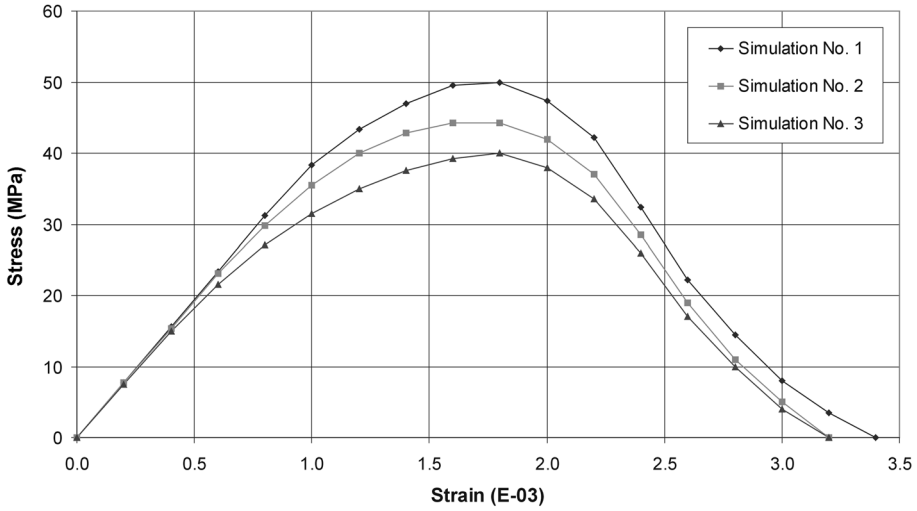

Fig. 5 Simulated stress-strain curve of concrete cube under compressive loading

perpendicular direction. The predicted stress-strain curves are shown in Fig. 5. The results indicate that the concrete specimens from all simulations behave almost linearly up to 30 percent of the ultimate load, and then are followed by a non-linear part. The degree of non-linearity increases with increasing displacement until the ultimate load is attained. Thereafter, the specimens soften and the load-carrying capacity gradually deteriorates until the specimen fails. It can be observed from all simulations that the magnitude of the peak stress increases when the material parameters of the interface phase are increased. The simulation for failure pattern of the specimen, when the interface is neglected, is presented in Fig. 6. The shear band type of cracking is observed, though the model considers only tensile failure at the micro-level. Most cracks propagate at the interface around aggregate particles. The values of the peak stress seem to be a proportion to the properties of interface.

Fig. 7 shows the stress-strain curves of concrete specimens simulated for different patterns of aggregate arrangement to consider the effect of the uncertainty in aggregate distribution. Four patterns of aggregate arrangement are considered. The arrangement in pattern 1 is the same as that in Fig. 1 and the fraction volume of aggregates is kept constant for all patterns. It is noted from Fig. 7 that the main difference in compressive behavior of concrete with different aggregate arrangement is the load-bearing capacity. The discrepancy in the ultimate loads of the specimens with well-

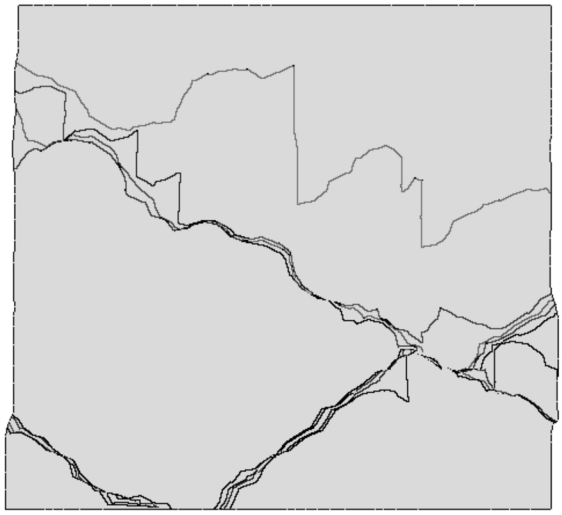

Fig. 6 Simulated crack pattern at failure of concrete cube under compressive loading

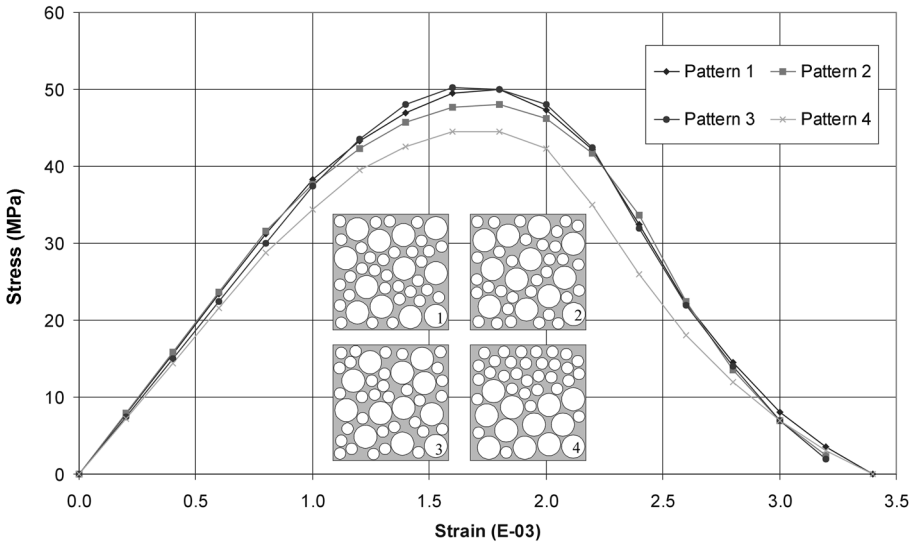

Fig. 7 Simulated stress-strain curves for different patterns of aggregate arrangement

distributed aggregate (pattern 1 to 3) is within five percent. The lowest ultimate load is found in the specimen of pattern 4, in which the segregation of aggregates occurs. Its value is about 10% lower than the average value of the other three patterns. The influence of the specimen size on the compressive behavior of concrete is investigated next. Fig. 8 presents the stress-strain curve simulated for three different sizes of a concrete cube. As expected, the predicted compressive strength is reduced when the specimen size is increased, which can normally be found in the experimental works.

The dependency of a finite element solution on the mesh size, or the so-called mesh sensitivity, is a serious problem usually found in a modeling stage. To check the mesh sensitivity for this model,

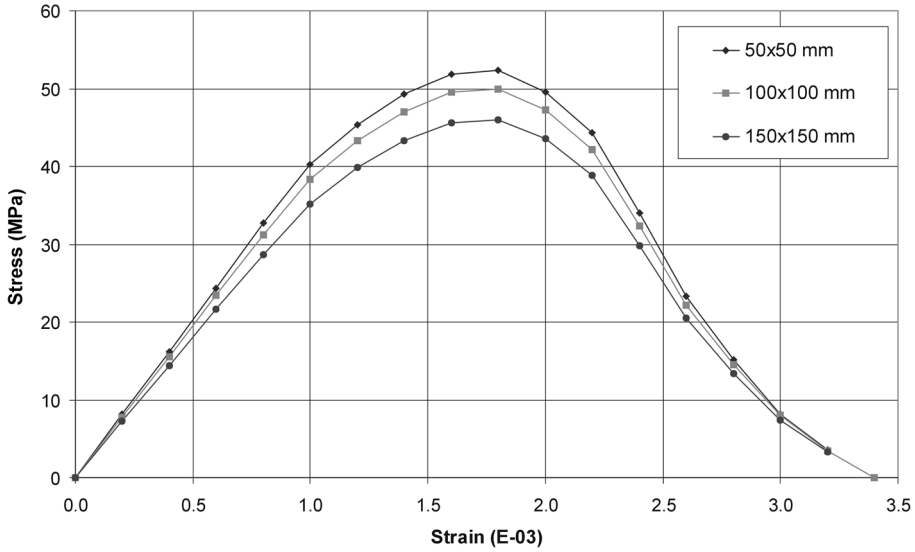

Fig. 8 Simulated stress-strain curves for different specimen sizes

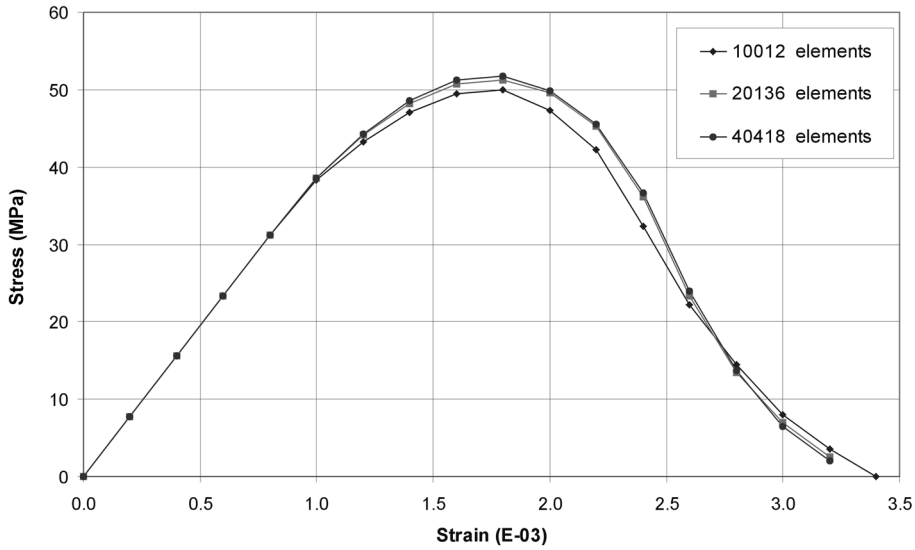

Fig. 9 Simulated stress-strain curves for different numbers of elements

three different discretizations are generated by using the same aggregate arrangement pattern and material properties. The number of element in each case are 10012, 20136, 40148 elements, respectively. It is evident from Fig. 9 that the model is mesh insensitive, provided that the mesh is fine enough to represent the heterogeneity in the concrete material.

Fig. 10 presents the comparison between stress-strain curves obtained from the present model and the truss-network model given by Mohamed and Hansen (1999b). Three mixes of a 100 × 200-mm concrete specimen with aggregate size of 19 mm are simulated. According to Mohamed and Hansen, the aggregate particles are assumed to be linear elastic throughout the simulation, i.e., only

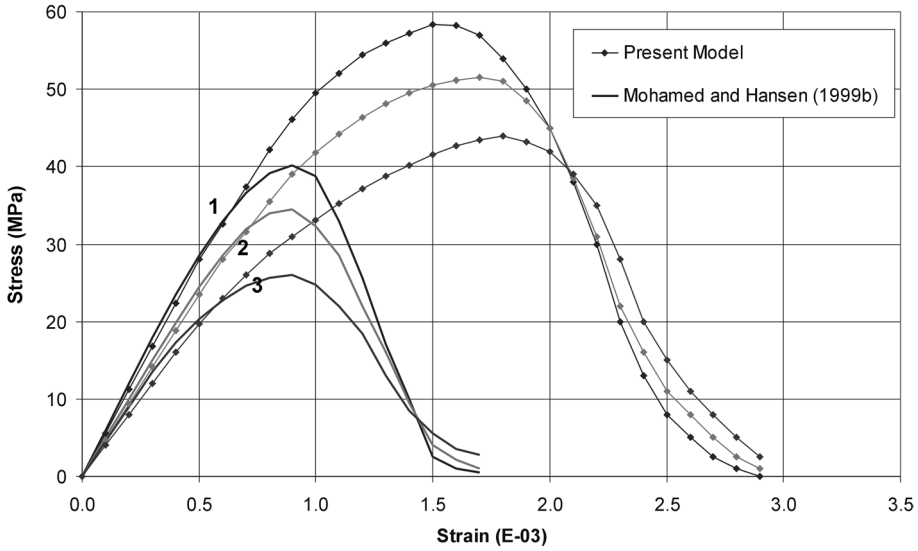

Fig. 10 Comparison of simulated compressive behavior with the truss-network model

Table 3 Material properties of each phase for comparison in Fig. 10

Simulation	Phase	E (GPa)	f_t (MPa)	G_F (N/mm)	ν
1	Matrix	40	8.0	0.080	0.25
	Interface	32	6.4	0.064	0.25
2	Matrix	35	6.0	0.080	0.25
	Interface	28	4.8	0.064	0.25
3	Matrix	30	4.0	0.080	0.25
	Interface	28	2.8	0.064	0.25

elastic modulus equal to 65 GPa is considered for the aggregate phase. The material parameters for the interface and matrix phases are given in Table 3. In addition, Poisson's ratio equal to 0.25 is used for both matrix and interface phases of all three simulations from the present model. Note that Poisson's ratio is not taken into account in Mohamed and Hansen's model.

Comparison in Fig. 10 indicates that the simulated ultimate load and the corresponding strain from both models are much different. The predicted ultimate loads of specimens from Mohamed and Hansen are lower and the corresponding strains are about 0.001. On the other hand, the predicted strains at ultimate loads from the present model are in the range of 0.0015-0.002, which are close to the typical value from the experiment. This may be a consequence of the fact that the model with truss elements has less loaded area than the one with the plane stress elements. When the concrete specimen is compressed, the truss elements will sustain higher stress and will fail prematurely. Since the failure criterion is defined in term of tensile strength, the ultimate load and the corresponding strain in the truss-network model will then be lower than those from the present model. In the next section, the compressive behavior simulated from the present model will be compared with the experimental results to validate the proposed model.

4. Model verification with experiment

The experimental work was performed at Chulalongkorn University to verify the accuracy of the present model. Three mixes of mortar were produced from the ordinary Portland cement, condensed silica fume, the river sand with fineness modulus of 3.04, the tap water, and the naphthalene-based superplasticizer, if necessary. The water/cement ratio was varied in order to make mortars with significantly different strengths. Only one type of crushed limestone with the maximum size of 20 mm was used as the coarse aggregate. The aggregate particles with the size less than 10 mm are about 60% of the whole aggregate by volume.

The tensile strength (f_t), elastic modulus (E), Poisson's ratio (ν), and fracture toughness (G_F) have been evaluated for mortar phase at the age of 28 days and aggregate phase as given in Table 3. Tensile strength of briquette mortar specimens was tested according to ASTM C-190, whereas for elastic modulus and Poisson's ratio, compression test of 50 × 50-mm cubic mortar specimens was performed. For the aggregate phase, the cored rock specimens with diameter of 10 mm were tested to evaluate their splitting tensile strength, elastic modulus, and Poisson's ratio, respectively. In addition, the fracture toughness was calculated for both mortar and aggregate phases according to the methods suggested by RILEM (1985) and ISRM (1988). The test setup for evaluating the fracture toughness of mortar is shown in Fig. 11. Due to the fact that the properties of the interface phase are extremely difficult to measure, they are assumed to be the same as those of the matrix phase. The high-strength concrete mixes had been made to ensure that the interface behaves well in the same degree as the bulk mortar (Monteiro and Mehta 1986).

Concrete was mixed and filled in 150 × 150-mm cubical molds prior to be demolded and stored in the water until the time of testing. The compression test of the concrete cube was performed at the age of 28 days by using the displacement-controlled universal testing machine. The axial deformation of the specimens was detected by dial gauges as shown in Fig. 12, which were removed after the highest load was achieved. Fig. 13 shows a comparison of the stress-strain curves between the numerical simulation from the present model and the experimental results. It is obvious

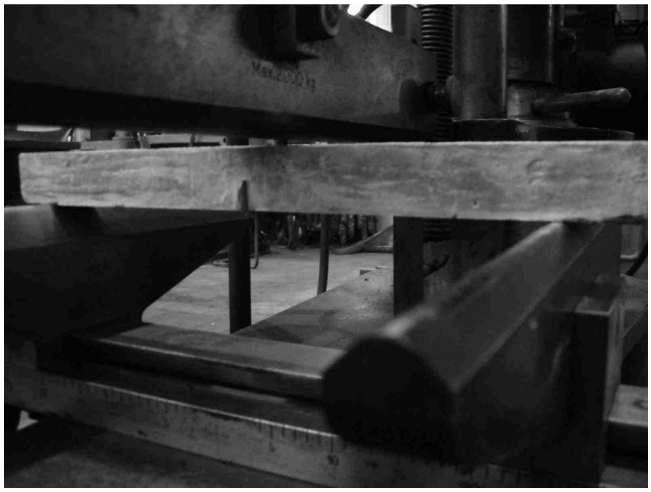

Fig. 11 Test setup for evaluating fracture toughness of mortar

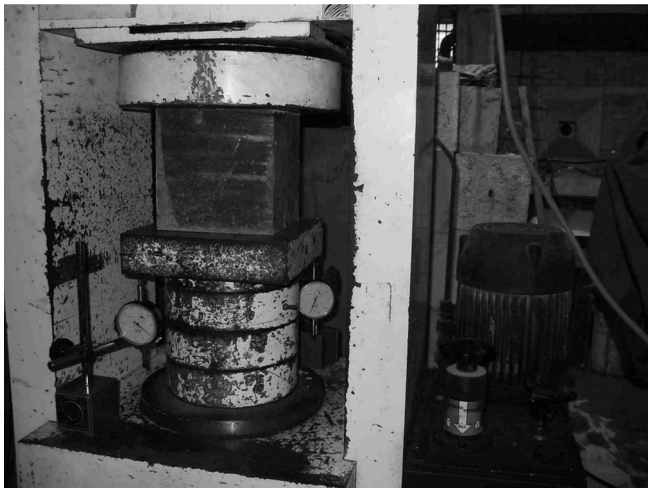

Fig. 12 Test setup for compressive test of concrete cube

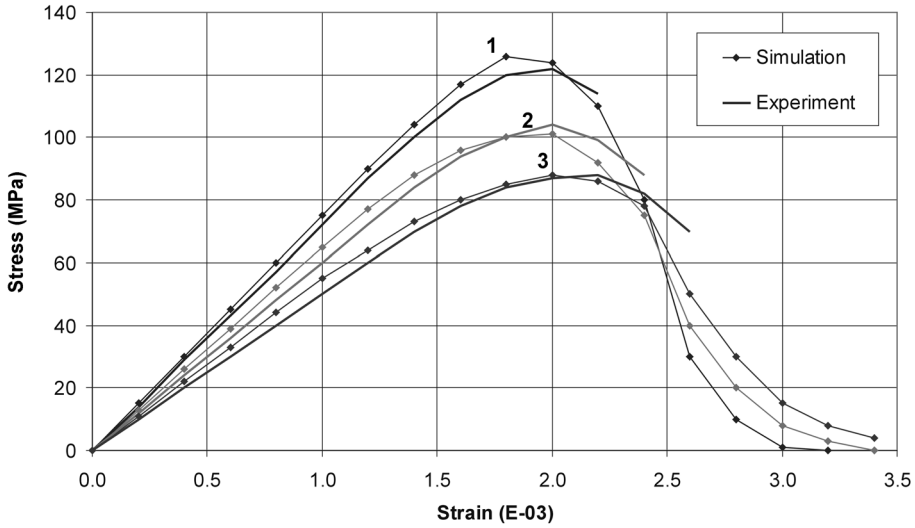

Fig. 13 Comparison of simulated compressive behavior with the experiment

Table 4 Material properties of each phase for comparison in Fig. 13

Mix No.	Phase	E (GPa)	f_t (MPa)	G_F (N/mm)	ν
1	Aggregate	98.2	20.8	0.09	0.17
	Matrix/Interface	38.5	9.2	0.07	0.24
2	Aggregate	98.2	30.8	0.09	0.17
	Matrix/Interface	36.8	7.8	0.06	0.24
3	Aggregate	98.2	20.8	0.09	0.17
	Matrix/Interface	27.6	5.2	0.06	0.25

Fig. 14 Typical failure of concrete cube under compressive loading

that a good agreement between the two results is obtained for both stiffness and strength characteristics of concrete in all three mixes. Fig. 14 presents the typical failure of the concrete cubes obtained from the experiment. Note that the shear band type of cracking is found as predicted from the present model (see Fig. 6).

5. Effect of component's tensile strength on concrete compressive strength

In this section, the influence of tensile strength of both aggregate and matrix phases on the compressive strength of concrete is presented. The same system used in the numerical results shown in Fig. 5 is employed in the parametric study to investigate this effect. The tensile strength of the aggregate phase is considered in the practical range of 8 to 40 MPa, whereas for the mortar phase, its tensile strength is varied from 2 to 16 MPa. Fig. 15 presents the influence of tensile strength from both phases to concrete compressive strength. It can be seen that increase in tensile strength of mortar phase raises the compressive strength of concrete. However, the increment in concrete compressive strength becomes smaller as the aggregate tensile strength is higher since the compressive strength is then controlled by the tensile strength of aggregate. Similarly, the improvement on concrete compressive strength by enhancing the tensile strength of mortar is also limited by the aggregate tensile strength.

Fig. 16 presents a chart for selecting appropriate values of aggregate and mortar strength to obtain desired concrete compressive strength. This chart may be applicable for concrete compressive strength up to 250 MPa, which is extremely high strength concrete. The experimental work has been carried out at Chulalongkorn University to demonstrate the applicability of the chart for the concrete strength higher than 150 MPa. Similar chart can also be developed to obtain a mortar with required strength from the appropriate values of the tensile strength of cement paste and fine aggregate.

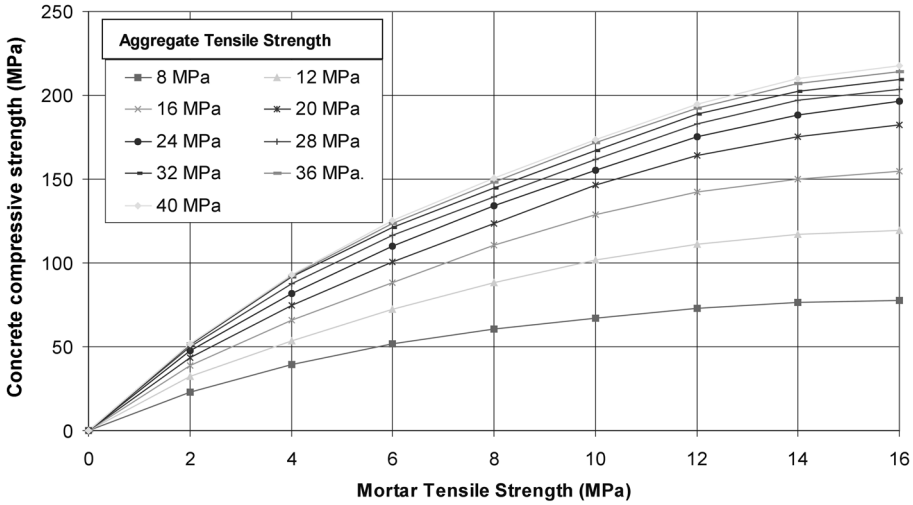

Fig. 15 Influence of tensile strength from mortar and aggregate on concrete compressive strength

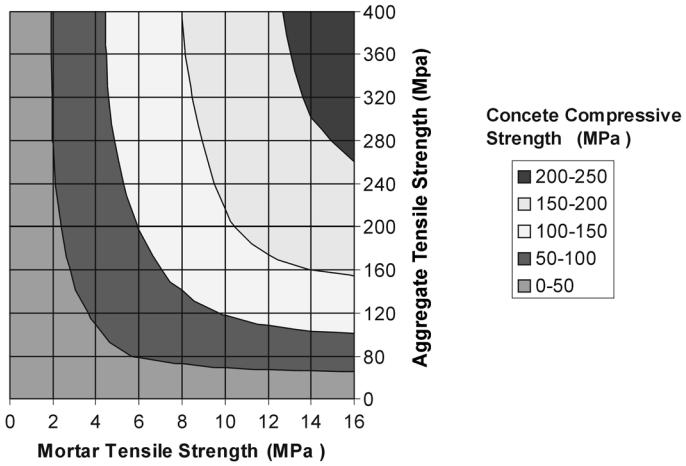

Fig. 16 Guideline on selecting component's tensile strength for specified concrete compressive strength

6. Conclusions

In this study, the micro-mechanical modeling of concrete microstructure to predict concrete behavior under compressive loading is presented. The concept of smeared crack approach of the fictitious crack model based on the non-linear fracture mechanics and the application of finite element method with the quadratic triangular element under plane stress condition is implemented. The proposed model can simulate the complete behavior of concrete under monotonic compressive loading, including the softening response and the cracking pattern at failure. The predicted stress-strain curves from the present model agree very closely with the experimental results. The incorporation of element size helps the model to be mesh-insensitive, i.e., the predicted response is

independent on the mesh size, provided that the mesh is fine enough to represent the internal heterogeneity. Furthermore, the effects of specimen size and aggregate arrangement pattern on the stress-strain curve can be observed. The contribution from the tensile strength of both aggregate and mortar phases to the compressive strength of concrete material is pointed out. The interaction diagram between the components' tensile strength and concrete compressive strength is established as a guideline to develop the concrete performance-based mix design. This model may be used for simulating the mechanical behavior of concrete material under other types of loading, such as, direct tension, shearing, or any combination of these actions. Nevertheless, the verification of the model for other loading types has to be performed.

Acknowledgements

The authors would like to thank the Thailand Research Fund (TRF) for providing financial support.

References

Bangash, M.Y.H. (1989), *Concrete and Concrete Structures: Numerical Modelling and Application*, Elsevier Applied Science, London.

Bazant, Z.P., Tabbara, M.R., Kazemi, M.T. and Pijauder-Cabot, G. (1990), "Random particle model for fracture of aggregate or fiber composites", *J. Engrg. Mech.*, **116**, 1686-1705.

Bazant, Z.P. and Oh, B.H. (1983), "Crack band theory for fracture of concrete", *Mater. Struct.*, **16**, 155-177.

Bazant, Z.P. and Planas, J. (1998), *Fracture and Size Effect in Concrete and Other Quasibrittle Materials*, CRC Press, Boca Raton.

Bazant, Z.P., Xiang, Y. and Prat, P.C. (1996), "Microplane model for concrete I. Stress-strain boundaries and finite strain", *J. Engrg. Mech.*, **122**, 245-254.

Cook, R.D., Malkus, D.S., Plesha, M.E. and Witt, R.J. (2002), *Concepts and Applications of Finite Element Analysis*, John Wiley & Sons, New York.

ISRM (1988), "Suggested methods for determining the fracture toughness of rock", *Int. J. Rock Mech. Min. Sci.*, **25**, 71-96.

Karihaloo, B.L. (1995), *Fracture Mechanics and Structural Concrete*, Longman, Harlow.

Kotsovos, M.D. (1987), "Consideration of triaxial stress conditions in design", *ACI Mater. J.*, **84**, 253-266.

Lorrain, M., Boukari, S. and Maurel, O. (1999), "Finite element analysis of high strength concrete beams: Modeling and validation", *Mater. Struct.*, **32**, 460-467.

Mohamed, A.R. and Hansen, W. (1999a), "Micromechanical modeling of concrete response under static loading – Part 1: Model development and validation", *ACI Mater. J.*, **96**, 196-203.

Mohamed, A.R. and Hansen, W. (1999b), "Micromechanical modeling of concrete response under static loading – Part II: Model predictions for shear and compressive loading", *ACI Mater. J.*, **96**, 354-358.

Monteiro, P.J.M. and Mehta, P.K. (1986), "Improvement of the aggregate-cement paste transition zone by grain-refinement of hydration products", *Proc. of the 8th Int. Congress on the Chemistry of Cement*, Vol. 3, Rio de Janeiro, 443-7.

RILEM Draft Recommendation (1985), "Determination of the fracture energy of mortar and concrete by means of three-point bend tests on notched beams", *Mater. Struct.*, **18**, 286-290.

Roelfstra, P.E. (1989), "Simulation of strain localization process with numerical concrete", *Cracking and Damage*, Mazars, J. and Bazant, Z.P. eds., Elsevier Applied Science, London, 79-90.

Schlangen, E. and van Mier, J.G.M. (1992), "Shear fracture in cementitious composites, Part II: Numerical simulations", *Fracture Mechanics of Concrete Structures*, Bazant, Z.P. ed., Elsevier Applied Science, New

York, 671-676.
Shah, S.P., Swartz, S.E. and Ouyang, C. (1995), *Fracture Mechanics of Concrete*, John Wiley & Sons, New York.
Wang, J., Navi, P. and Huet, C. (1993), "Application of fracture mechanics to the study of crack propagation in concrete structures using a granular microcracked model", *Fracture and Damage of Concrete and Rock*, H.P. Rossmanith, ed., E&FN Spon, London, 176-185.
Zaitsev, Y.B. and Wittmann, F.H. (1981), "Simulation of crack propagation and failure of concrete", *Mater. Struct.*, **14**, 357-365.
Zhong, X. and Chang, C.S. (1999), "Micromechanical modelling for behavior of cementitious granular materials", *J. Engrg. Mech.*, **125**, 1280-1285.
Zubelewicz, A. and Bazant, Z.P. (1987), "Interface element modeling of fracture in aggregate composited", *J. Engrg. Mech.*, **113**, 1619-1630.